Separated Hypersonic Turbulent Flow Measurements on Spoilers

R. Berman,* A. Hecht,† J. Metzger,‡ and D. Nestler§
General Electric Company, Philadelphia, Pa.

Results are presented for a test program that measured heat transfer, pressure, and drag for a variety of spoiler geometries in hypersonic turbulent flow. Techniques are described whereby such measurements were made simultaneously on three spoilers mounted at the rear of a 6.3° half angle cone having bluntness ratios of 0, 0.082, and 0.164. Spoiler geometries include variations in height, angle, and contour which are thought to be representative of ablated shapes. Nominal freestream test conditions were Mach 11 and Reynolds number of 20×10^6 based on model length. Heat flux and pressure distributions along spoilers of different geometry are shown to correlate when plotted vs a distance coordinate normalized by the distance to maximum heat flux and pressure, respectively. The magnitudes of maximum heat flux and pressure are compared with current prediction techniques. Based on these comparisons, improved prediction methods are suggested that will enhance the ability to predict spoiler performance during re-entry deployment.

Nomenclature

C_A = axial force coefficient
H = spoiler height; also enthalpy
h = heat-transfer coefficient
L = model length
L_s = length of separated shear layer
M = Mach number
n = exponent in pressure correlation of maximum heat flux
p = pressure
$\dot{q}$ = heat flux
R_B = base radius
R_N = nose radius
R_{∞_L} = Reynolds number based on freestream conditions and L
St = Stanton number
t = time
u = streamwise velocity
X = distance along spoiler face from base of spoiler
X_M = distance from spoiler base to point of maximum heating
X_0 = distance from stagnation point to base of spoiler
X_s = distance from stagnation point to separation
α = angle of attack
Δ = distance along model surface from separation to spoiler base
δ_f = spoiler angle measured from model surface
δ'_f = spoiler angle measured from model centerline
δ_s = separation angle
δ_l = thickness of separated shear layer
θ_s = shock angle
ρ = density
μ = viscosity

Subscripts

0 = condition on cone surface without spoiler
1,2,3 = regions of flow: before separation, in separated region, after reattachment
max = maximum value
R = recovery value
ref = reference value on 0.5-in.-radius sphere
w = wall value
∞ = freestream value

Presented at the AIAA 9th Aerodynamic Testing Conference, Arlington, Texas, June 7-9, 1976; submitted July 6, 1976; revision received Oct. 28, 1976.

Index categories: Boundary Layers and Convective Heat Transfer – Turbulent; Entry Deceleration Systems and Flight Mechanics.

*Project Engineer.
†Senior Engineer, Aerothermodynamics.
‡Supervisor, Experimental Engineering. Member AIAA.
§Consulting Engineer, Aerothermophysics. Member AIAA.

Introduction

THE successful recovery of re-entry vehicles using spoilers for rapid deceleration critically depends upon the shape change characteristics of the spoilers during the recovery phase. The shape of the spoiler in flight may be changed by the combined effects of thermochemical and thermomechanical ablation. Since considerable uncertainty exists in defining the respective contributions of these two mechanisms, the present program was undertaken to provide data necessary to develop improved definition of spoiler heat flux and pressure distributions.

At the outset of the program, semiempirical techniques existed to compute peak reattachment heating on deflected surfaces; however, an undesirably large data scatter existed. Furthermore, data were available only for straight spoiler shapes with limited height and angle variations. Large discrepancies existed between different methods of approximating spoiler pressure for blunt-nosed cones. The present program was planned to provide spoiler heat flux, pressure, and drag data for a variety of spoiler geometries considered representative of ablated shapes. These drag data made use of a new balance capability that allows direct measurement of spoiler drag in the presence of the forebody.

Test Model

Experimental data were generated on a model consisting of a 6°18′ half angle cone to which the various spoiler configurations were affixed. A representative view of the assembled model is given in Fig. 1. The body consists of four sections. The nosetip section is comprised of two separate components for sharp and blunt nosetips. The nosetip configurations employed in the program are enumerated in Table 1. These components assembled to the body of the cone, which comprises the second section of the test specimen. It is split longitudinally into two half cones to provide more convenient access to the interior of the specimen for handling instrumentation leads. The third section of the model is a conic ring, which constitutes the most rearward portion of the

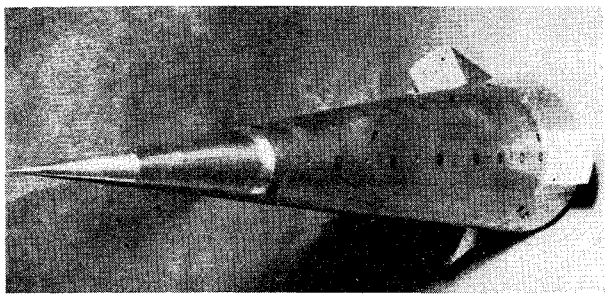

Fig. 1 Assembled test model.

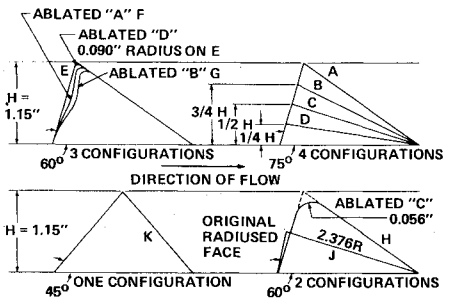

Fig. 2 Compilation of spoiler profiles tested.

specimen. It provides a continuous structure into which the sets of spoilers are installed. In the present design, one of the three locations provided for spoiler installation was modified to accept a special lightweight spoiler assembly installed in conjunction with a strain-gage force balance system. The modified location alternately was fitted with a spoiler containing an array of heat-transfer gages. This array was tested in place of the heat-transfer array, which constituted the instrumentation on another of the spoilers during some selected tests.

The spoilers employed in the program represented eleven different variations in geometry (see Fig. 2). Although in actual application the initial (unablated) spoiler shape is curved, the straight shape was selected as a more fundamental shape on which to perform angle and height perturbations. The straight shape was also regarded as representative of an ablated spoiler shape, based on ballistic range test results.

The basic cone geometry for the majority of the tests was selected to be the sharp cone ($R_N/R_B = 0$), in order to provide natural turbulent flow upstream of flow separation. A sharp cone also provides better-defined flow properties upstream of separation than a blunt cone, thereby constituting a more fundamental condition with which to verify prediction methods. Actual flight applications involve blunt noses; therefore, two additional noses of 0.185 and 0.370 in. radius were also used, corresponding to bluntness ratios R_N/R_B of 0.082 and 0.164. It was necessary to install trip rings on these noses (see Table 1) to produce turbulent flow ahead of separation.

The array of sites for instrumentation was laid out in a staggered pattern, the basic geometry of which was employed for all spoilers. The alternate heat-transfer site arrays on spoiler number three use the same pattern, translated half a gage pitch. This was done to provide better resolution of heat-transfer maxima. When the flow proved to be very nearly axisymmetric and repeatable, these data were coplotted with those of spoiler number one to give a more detailed picture of the distribution of heat transfer on the face of the spoiler.

The model was equipped to obtain data in three categories. First, heat-transfer measurements were obtained using two types of gages. Second, pressure was measured employing two types of sensors covering three ranges. Finally, strain gage instrumentation was introduced to obtain drag measurements.

Of the two types of heat-transfer gages, the body of the model was equipped with the "thin-skin calorimeter," which depends on the backface response of a very thin metal plate. The spoilers were instrumented with chromel-constantan coaxial surface thermocouples. These thermocouples are

Table 1 Nosetip configurations tested

		Nosetip trips		
No.	R_N/R_B	Radius, in.	Ring diam, in.	Bead diam, in.
1	0	0.001	none	none
2	0.082	0.185	0.380	0.020
				0.0393
3	0.164	0.370	0.748	0.020
				0.0393

unique in that the dissimilar metals themselves comprise the heat-transfer gage. A rod of chromel material coated with an electrical insulator several mils thick is press fitted into a hollow cylinder of constantan. The cylindrical assembly thus formed is treated as an infinite slab and one-dimensional heat-transfer analysis is applied to the evaluation of the thermal flux. At installation, it is thermally and electrically insulated from the body of the spoiler by a thin cylindrical shell of Lexan.

The coaxial surface thermocouples were contoured to match the spoiler surface if curved. All gages were calibrated prior to their installation. The gages covered a range of 30 to 300 BTU/ft^2 sec.

Model pressures were measured with two types of internally mounted pressure transducers: a miniature semiconductor strain-gage-type ¼ in. diam and 0.6 in. long, and a wafer-style semiconductor strain-gage-type 0.6 in. diam and ¼ in. thick. Wafer gages of 0.15 to 30 psid range were used in the conical model forebody. Wafer gages of 1 to 100 psid range and miniature semiconductor strain-gage types of 1 to 100 and 3 to 300 psid were used in the spoilers. All gages were operated in their optimum measuring range.

During a portion of the test, aerodynamic forces were measured on one spoiler by mounting a small three-component force balance directly below the spoiler. The balance load cells were instrumented with semiconductor strain gages, and semiconductor accelerometers provided compensation for model inertial loads that result from vibrations of the model and its support hardward. The balance was calibrated in the AEDC-VKF Balance Calibration Laboratory before use in the tunnel.

Facility/Test Program

The Hypervelocity Wind Tunnel F at the Arnold Engineering Development Center is an arc-driven wind tunnel of the hotshot type and capable of providing Mach numbers from approximately 7.5 to 22 over a Reynolds number per foot range from 0.05×10^6 to 75×10^6.

This test was conducted in the 54-in.-diam test section of the conical nozzle for $M_\infty = 10.8$. Nitrogen was the test gas. The 4.0 ft^3 arc chamber was used, and useful test times up to approximately 200 msec were obtained. To achieve the required operating conditions, an initial charging pressure of 260 psi was employed in the arc chamber. At firing, the electrical current discharged through the arc chamber reached a maximum of 570,000 A.

For all runs, the three spoilers were identical in configuration, i.e., shape, angle, and height. Spoiler No. 1 was always used to measure the heat-transfer rate, Spoiler No. 2 was always used to measure pressure, and Spoiler No. 3 was used in the first part of the test for heat-transfer-rate measurements and was then converted to force measurement for the last part of the test.

Spoiler Heat Flux

The spoiler heat flux graph (Fig. 3) provides detailed heating distributions that are remarkably consistent for reat-

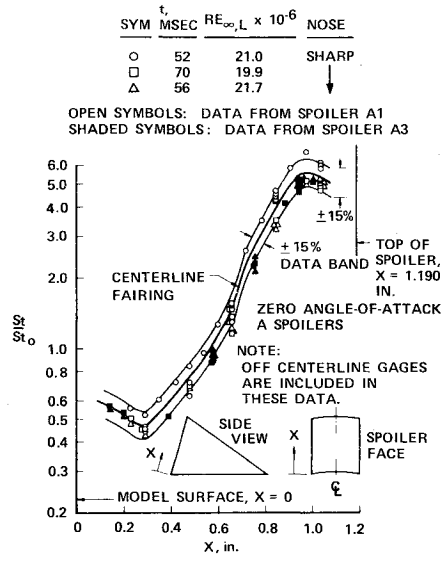

Fig. 3 "A" spoiler heat-transfer distributions.

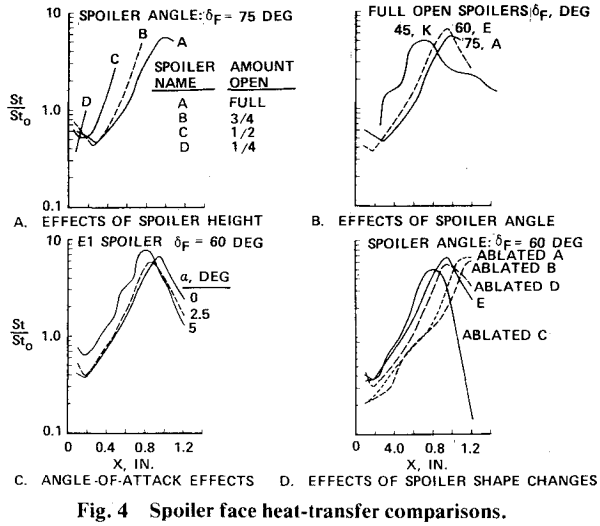

Fig. 4 Spoiler face heat-transfer comparisons.

tachment heating measurements. The technique of superimposing data of staggered instrumentation from two different spoilers for the same run appears to have been successful in providing better resolution of the steep gradients and heating maxima characteristic of reattachment regions. The absence of severe spanwise gradients also permits the use of data from different gage columns (of differing spanwise location) to define chordwise distributions with more clarity than normally possible.

A summary of spoiler heating distribution, as shown in Fig. 4, produces several interesting observations:

1) For those configurations having a clearly defined heating maximum, the ratio of St/St_0 is relatively insensitive to spoiler angle or shape, varying between values of 5 to 7 for $R_N/R_B=0$ and 4 to 5 for $R_N/R_B=0$. Since the undisturbed cone heat flux is 0.1 of $\dot{q}_{\text{ref}}$, the values of $\dot{q}_{\max}/(\dot{q}_0)_{\text{cone}}$ ranges from 50 to 90.

2) Heating distributions have remarkably similar shapes for the various configuration changes. This observation suggested that $\dot{q}/\dot{q}_{\text{ref}}$ be plotted vs a normalized coordinate X/X_M, in which X and X_M are the distances from the spoiler base to the location of local and maximum spoiler heat flux, respectively. For those configurations not showing a heating maximum in the data, it was assumed that the maximum occurred at the spoiler tip. In Fig. 5, the centerline data for the 75° spoiler are plotted in this fashion for four different

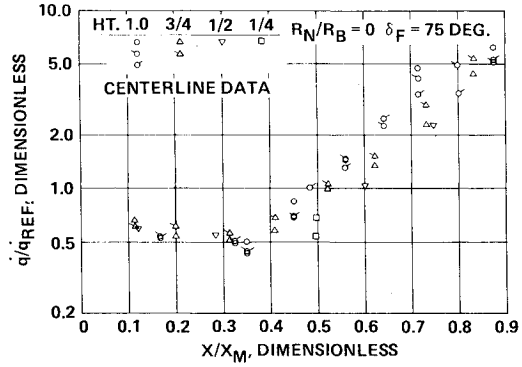

Fig. 5 Effects of spoiler height on heat-flux distribution.

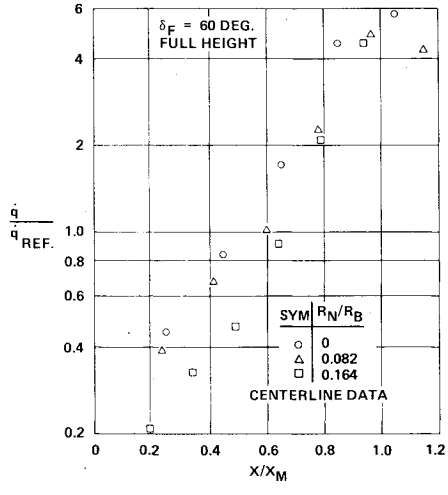

Fig. 6 Effects of R_N/R_B on heat-flux distribution.

spoiler heights. The data group reasonably well, suggesting that the low values of $\dot{q}/\dot{q}_{\text{ref}}$ measured on the ½ and ¼ height spoilers are primarily due to the gage placement from the spoiler tip being a larger fraction of the total spoiler height. In Fig. 6, the centerline data for the 60° spoiler are plotted vs X/X_M for the three nose bluntnesses. Again, the data group well, although the larger nose bluntness case has somewhat reduced heating for $X/X_M<0.7$. In Fig. 7, the centerline data for the four "ablated shapes" are plotted vs X/X_M, together with the 60° straight full height spoiler data. The type of ablated shape is seen to have little effect on the heating distribution, although large shifts in peak heating location exist among the shapes. In Fig. 8, the centerline data for the full height straight spoiler are plotted vs X/X_M for spoiler angles of 75°, 60°, and 45°, again confirming the "universal distribution" concept. The half-height original shape and half-height 75° straight spoiler also have similar heating and pressure distributions.

3) Although the spoiler heat flux distributions have similar shapes, the location of maximum heat flux X_M (which anchors the distribution when plotted vs X/X_M) is sensitive to changes in spoiler height, angle, and shape. Values of X_M are tabulated in Table 2 for all $\alpha=0$ cases for which a maximum in heat flux could be defined from the heating distributions. For all other cases, the maximum is assumed to occur at the spoiler tip.

4) For spoiler angles of 60° and 45°, the location of maximum heat flux is far enough inboard from the tip to define a region of rapid decrease in heat flux outboard of the maximum, followed by a region of less rapid decrease (see Fig. 4B). This type of heat-flux distribution would create an ablated shape of the cusped type (ablated shapes A or B) if it persisted; however, the effect of a cusped shape is to shift the

Table 2 Location of maximum heat flux

R_N/R_B	Spoiler height	Spoiler angle Δ_F, deg	Spoiler shape	Location of max. heat flux X_M, in.
0	Full	75	Straight	1.0
0	Full	60	Straight	0.93
0	Full	45	Straight	0.71
0	–	–	Ablated A	1.125
0	–	–	Ablated C	0.78
0	–	–	Ablated D	0.95
0.082	Full	60	Straight	1.02
0.164	Full	60	Straight	1.25
0.164	Full	45	Straight	1.01

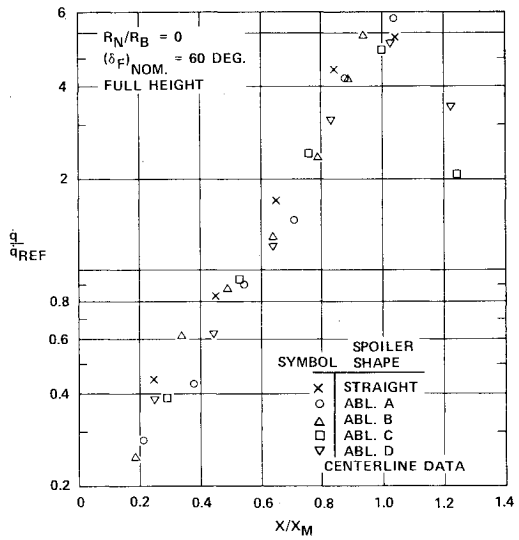

Fig. 7 Effects of spoiler shape heat-flux distribution.

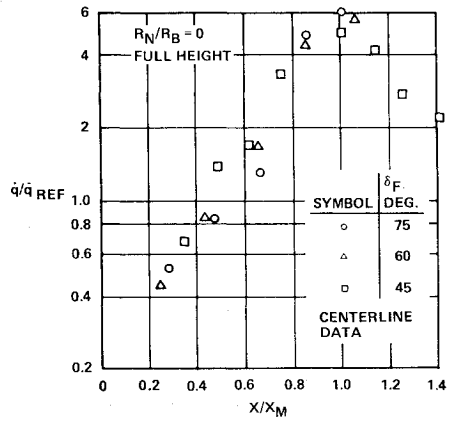

Fig. 8 Effects of spoiler angle on heat-flux distribution.

location of maximum heat flux further outboard relative to a straight shape. This sensitivity of heat-flux distribution to shape change is clearly a major obstacle to the development of a "simplified yet accurate" spoiler-ablation model.

Reattachment Heating Prediction Technique

The method used to calculate the spoiler reattachment turbulent heat flux was based on a modification of a correlation equation for peak heating for separated-reattachment turbulent heat transfer derived by Bushnell and Weinstein.[2] The flow separation model, with the important variables in the regions of interest, is shown in Fig. 9. The equation used to calculate the peak reattachment heating is

$$\frac{h_{max}}{\rho_w u_3} = 0.0415\left[\frac{\rho_w u_3 \delta_t}{\mu_w \sin(\delta_F - \delta_s)}\right]^{-0.2} \quad (1)$$

For axisymmetric flow, δ_t is computed by multiplying the expression given by Bushnell and Weinstein for planar flow by the factor 0.524 derived by Walker[3] for conical boundary-layer growth.

Bushnell and Weinstein derived the form of Eq. (1) by correlating reattachment heating for values of $(\delta_F - \delta_s)$ between 15° and 45°. Experimental data for higher values of relative flow angles $(\delta_F - \delta_s)$ (e.g., Ref. 4) were correlated and they indicated a higher level of heating than given by Bushnell and Weinstein. Consequently, the constant of Eq. (1) was selected to reflect this increased heating.

The flow properties behind the reattachment shock are calculated by first evaluating the properties behind the separation shock, using the correlation of separated region pressure given by Kaplan[5] and applied by Nestler.[6] Given the

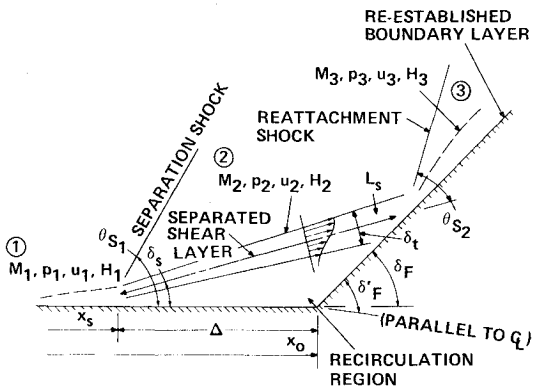

Fig. 9 Separation/reattachment flow model.

properties in region 1 (Fig. 13) and p_2, the separation angle may be calculated. Treating this as a ramp or wedge angle, the separation shock angle and subsequently the conditions in region 2 may be found. For blunt cone configurations, these upstream properties vary normal to the body surface, ranging between gas at the stagnation point entropy to flow properties associated with traversal of an essentially conical shock. Thus, the state of the upstream flow is a basic uncertainty in the analysis.

The conditions in region 3 are dependent upon the reattachment shock angle, measured with respect to the shear layer centerline in Fig. 9. For values of $(\delta_F - \delta_s)$ up to approximately 45°, this reattachment shock angle is considered as an attached shock on a wedge. Beyond a limiting spoiler angle the shock becomes detached and is theoretically 90° at the shear layer centerline. In reality, however, the reattachment shock is curved. This difficulty in defining the effective reattachment shock angle, along with the uncertainty of the flow properties that are entrained in the shear layer for

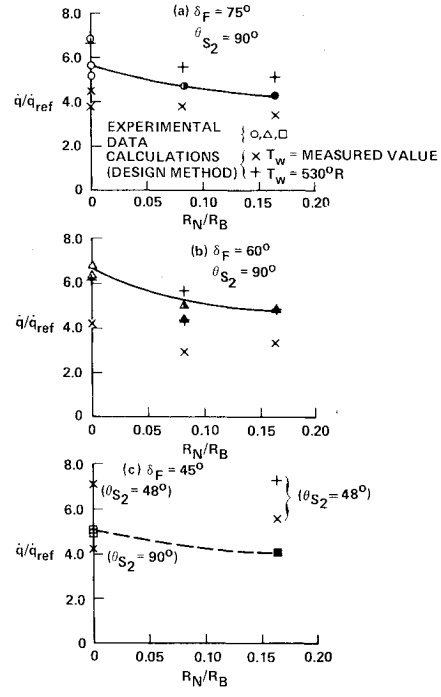

Fig. 10 Peak heating ratio vs bluntness ratio.

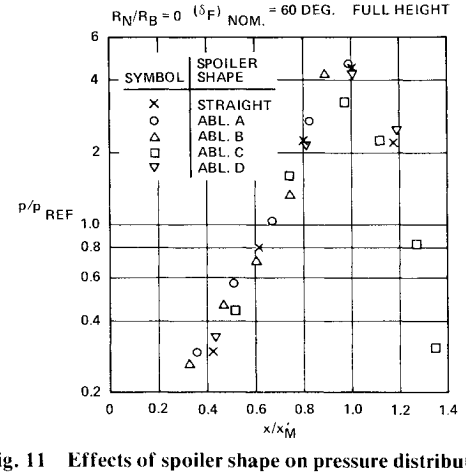

Fig. 11 Effects of spoiler shape on pressure distribution.

blunt nosed configurations, are probably the two most important contributions to prediction uncertainty for spoiler reattachment heating. Definition of the separation angle and length are of importance in predicting the point of maximum heating but are not of overriding importance in predicting the absolute level of heating.

Predictions of maximum spoiler heat flux were made for selected configurations, using Eq. (1) to determine h_{max}. The wall properties (ρ_w, μ_w) were based on the actual gage temperature at the test time corresponding to the heat-flux data. The predicted heat flux is then given by

$$q_{max} = h_{max}(H_R - H_w) \tag{2}$$

in which the wall enthalpy H_w was based on $(T_w)_{max}$. No attempt was made to correct the predictions for nonisothermal wall effects on boundary-layer development or for conduction errors.

The predicted maximum spoiler heat flux was found to be a very sensitive function of the assumed properties just ahead of separation in the case of the $R_N/R_B = 0.164$ configurations. The calculated levels varied considerably depending upon whether the flow was expanded to local pressure from a

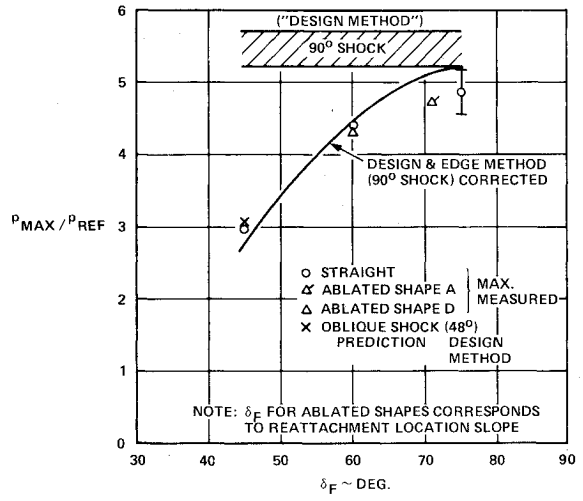

Fig. 12 Maximum pressure predictions for $R_N/R_B = 0$.

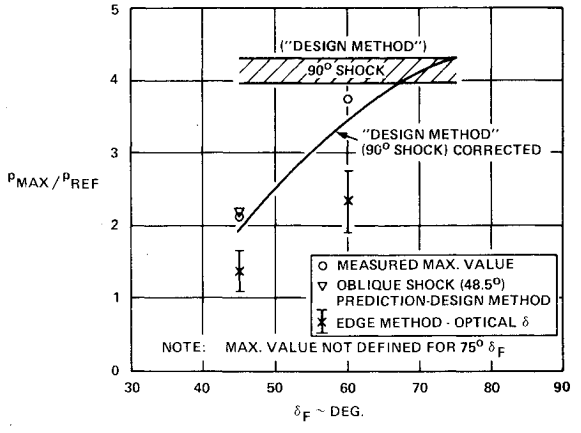

Fig. 13 Maximum pressure predictions for $R_N/R_B = 0.164$.

conical shock (design method), or whether the properties were evaluated by determining the boundary-layer edge from test films and using a flowfield property calculation at the observed edge of the boundary layer (edge method). For the $R_N/R_B = 0.082$ bluntness ratio, however, the differences in predicted heating rates between the two methods were small. This indicates that the $R_N/R_B = 0.082$ bluntness had essentially reached conical flow at separation, whereas the $R_N/R_B = 0.164$ bluntness influenced the flow at this point.

Figure 10 shows the decrease in peak $\dot{q}/\dot{q}_{ref}$ vs R_N/R_B for $\delta_F = 75°$, 60°, and 45°. Figure 10 also includes the calculated peak heating rates using the design method. For the 75° and 60° spoilers the design method using the measured wall temperatures underpredicts peak heating, whereas for the 45° case the method overpredicts for $\theta_{S_2} = 48°$. Calculations were also made using the initial spoiler temperature, since it has been found that the design method is very sensitive to wall temperature due to the use of wall values of density and viscosity in the prediction technique. Use of an initial temperature of 530° R slightly overpredicts the 75° spoiler heating and gives good results for the 60° spoiler. As would be expected, the 45° spoiler rates are much too high using this method, since the actual wall temperature predictions were already high.

Three conclusions may be made from Fig. 10: 1) The wall temperature is not a good basis for evaluating the properties to be used in the heating correlation since the predicted heating rates are much too sensitive to changes in T_w. Since past experience has indicated that a reference enthalpy approach has been an excellent basis for calculating boundary-

layer heating rates, it is recommended that this approach be used in reattaching flow to avoid the sensitivity problem encountered here. 2) Assuming that the major cause of the error in predicting the heat flux is the sensitivity of the prediction to wall temperature, it would appear that the flow over the 75° and 60° spoilers is predominantly conical, perhaps due to the thickening of the boundary layer caused by the trips. The 45° spoiler is below the conically controlled heating prediction, and the boundary-layer edge prediction and the conical prediction bound the measured results. 3) For prediction of heating rates it appears that the 90° shock assumption for 75° and 60° spoiler angles is somewhat too high, and an oblique attached shock is too low for the 45° spoiler. The effective angle for evaluation of heat transfer is somewhere in between these limiting values and must be found by empirical means.

Spoiler Pressure

The measured spoiler pressure distributions are quite consistent with the spoiler heat-flux distributions. For configurations having a clearly defined maximum in pressure, the location of this maximum is slightly outboard (by 0.030 to 0.080 in.) of the location of maximum heat flux. This is consistent with the findings of Holden[7] for two-dimensional ramp separation studies at $M_\infty = 6.5$-13.

Due to the similarity between spoiler pressure and heat-flux distributions, the same observations made previously under "Spoiler Heat Flux" apply to the pressure distributions. For example, the concept of a universal spoiler pressure distribution (similar to the universal heat-flux distribution noted above) is verified in Fig. 11. In this figure, centerline pressure data for the four "ablated shapes" are plotted vs X/X'_M, together with the 60° straight full height spoiler data. In Fig. 11, X'_M is the estimated location of maximum pressure, as determined from the pressure data plots for the respective configurations. The type of ablated shape is seen to have little effect on the pressure distribution, although large shifts in peak pressure location exist among the shapes. The only significant exception to the "universal distribution" concept appears to be the case of $\delta_F = 45°$ for $R_N/R_B = 0.164$.

Pressure Predictions

Calculations were made to predict the peak pressure on the spoiler front face, as well as the cone surface pressure prior to separation and the "plateau pressure" within the separated flow region. The technique used to predict the separated flow properties in Region 2 (Fig. 9) has been described under "Reattachment Heating Predictions." For $R_N/R_B = 0$, these flow properties are well defined, since little variation occurs from the body surface to the bow shock wave. For $R_N/R_B \neq 0$, however, significant variation of properties occurs across the shock layer, creating an uncertainty in flow conditions approaching the spoiler. As discussed above, two methods have been used: "design method" and "edge method." These methods give identical results for $R_N/R_B = 0$, but yield divergent results for $R_N/R_B \neq 0$. One of the objectives of the present program was to determine which, if either, method was preferable for predicting maximum spoiler pressure.

In either method, the reattachment shock angle must be assumed in order to compute flow properties in region 3 (Fig. 9). For flow reattachment angles greater than 45°, no attached oblique shock solution exists; hence, a reattachment shock angle of 90° has been assumed. For flow reattachment angles less than 45°, the Bushnell-Weinstein method suggests the use of a reattachment shock angle corresponding to the oblique shock associated with the approach flow of region 2 (Fig. 9) and a turning angle of $\delta_F - \delta_s$.

Comparison of predictions using 90° reattachment shock angles with measured maximum spoiler pressures for $R_N/R_B = 0$ showed an overprediction which increased as the spoiler angle decreased. Therefore, a correction was applied to the peak pressure computed from the normal shock assumption, as a factor p/p_t which is a function of flow turning angle $\delta_F - \delta_s$. This correction for effects of turning angle was derived using empirical data correlations together with theoretical calculations (see Refs. 8-10).

The results of the comparison of predicted vs measured maximum spoiler pressure are summarized in Figs. 12 and 13. In Fig. 12, the sharp cone results ($R_N/R_B = 0$) are plotted vs spoiler angle δ_F. The "design method" predictions based on a 90° reattachment shock clearly overpredict the measured maximum pressures for $\delta_F = 45°$ and 60°. However, the corrected design method is in good agreement with measured results. The oblique shock prediction for $\delta_F = 45°$ also matches the data well. In Fig. 13, the larger bluntness results ($R_N/R_B = 0.164$) also agree well with the "design method." The edge method appears to underpredict the data, whereas the design method slightly overpredicts. Since considerable uncertainty in true boundary-layer thickness exists for the blunt cones due to interpretation of the optical data, a conclusive preference for the modified design method cannot be justified on the basis of these results. The large thickening of the boundary layer caused by the trips produces an altered separated flowfield, which is not representative of a naturally turbulent flow of the same R_N/R_B. The trips have caused the reattaching flow to be closer to "conical" conditions, thus implicitly favoring the "design method" over the "edge method." The correct way to predict spoiler pressures for a nonsharp cone in flight remains unresolved, due to inherent ground test facility limitations.

Spoiler Drag

In addition to the temperature and pressure measurements, axial force measurements were made for selected spoiler configurations. These data reflect a first in that the ΔC_A due to a spoiler was measured directly. Previously, the C_A of the total cone configuration with and without spoilers had to be measured, the axial force due to the effect of flow separation on the cone surface pressure was subtracted, and then the residual axial force was divided by the number of spoilers (three). These tests were conducted for the 0, 0.082, and 0.164 nose bluntness configurations with the basic 60°, full open spoilers. The various "ablated shapes" were also tested for the sharp nosetip. Figure 14 presents the results of these tests. Indicated are the spoiler profiles for each run, the test data band, and the predicted values. As shown, the predicted ΔC_A is about 15% lower than measured for the 60° straight and ablated shape D spoilers for $R_N/R_B = 0$, and the 60° straight spoiler for $R_N/R_B = 0.082$. For the 0.164 bluntness, the prediction for the 60° straight spoiler is slightly higher than measured. One disturbing indication is shown in the comparison of the ablated shape A, B, and C spoilers. For a slight change in front face profile (ablated A vs ablated B), there is a significant variation in the measured ΔC_A for these two shapes; whereas the prediction technique indicates a much smaller change. The ablated C configuration shows little

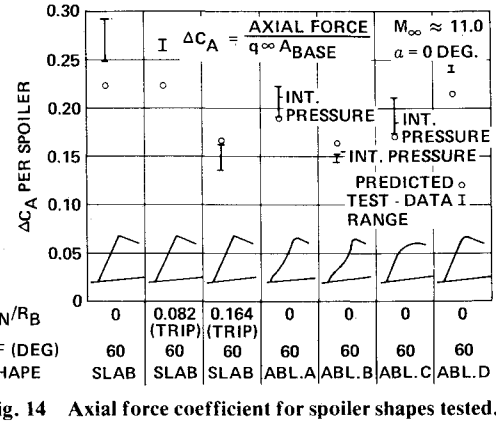

Fig. 14 Axial force coefficient for spoiler shapes tested.

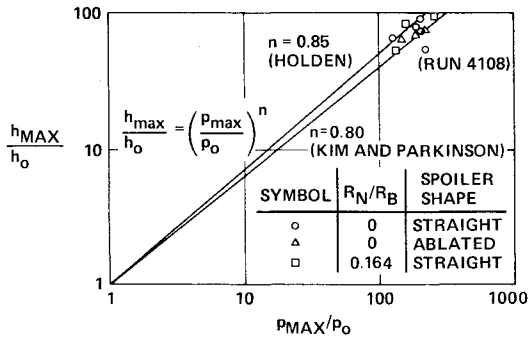

Fig. 15 Correlation of maximum heat-transfer coefficient with maximum pressure.

difference in ΔC_A from the ablated A value. Integration of the measured pressure data indicate agreement with the force measurements for the A, B, and C configurations. Consideration of the similar shapes of the pressure distributions for the various spoiler shapes, as demonstrated earlier in Fig. 11, indicates that the variation in spoiler drag between ablated shapes A and B is associated with the outward shift in the reattachment location for shape B due to its steeper slope near the tip.

Correlation of Spoiler Heat Transfer with Spoiler Pressure

Several previous investigators have empirically correlated maximum reattachment heating for turbulent flow with maximum reattachment pressure, using the relation

$$h_{max}/h_0 = (p_{max}/p_0)^n \qquad (3)$$

The quantities h_{max} and p_{max} are the maximum reattachment heat transfer coefficient and pressure, while h_0 and p_0 are the "undisturbed" heat-transfer coefficient and pressure upstream of separation. Various values of n have been reported; the most popular values are $n=0.85$, obtained by Holden[7] in a study of two-dimensional flat plate-ramp separation, and $n=0.80$, obtained by Kim and Parkinson[11] in a study of a cone-flap configuration. In these studies, the flow turning angles did not exceed 36°.

The present results were converted to the form required by Eq. (3) and are plotted in Fig. 15 for all runs for which p_{max}, $\dot{q}_{max}$, and h_0 could be determined with reasonable accuracy. Also shown are the correlation lines corresponding to $n=0.85$ and 0.8. The present data are seen to group between values of $n=0.80$ and 0.86, with one exception which is inexplicably low.

Since the correlation of Fig. 15 appears to hold for the various spoiler shapes tested under the present program, a simple method suggests itself for predicting maximum spoiler heat-transfer rates from a knowledge of maximum spoiler pressure. Thus, if an accurate method of predicting maximum reattachment pressure can be evolved, Fig. 15 offers an extremely simple way to predict maximum heat transfer to within +20%.

Conclusions

The techniques described herein for the simultaneous measurement of heat transfer, pressure, and drag of individual spoilers have provided data useful in the development of spoiler design techniques for recovery of hypersonic re-entry vehicles. Of particular interest is the effect of various ablated spoiler shapes on the heat transfer, pressure, and drag.

The principal remaining uncertainty in predicting spoiler environment for re-entry is the effect of nose bluntness on local flow properties along the spoiler. Future tests require a naturally turbulent boundary layer on a blunt-nosed model to resolve this question.

Acknowledgment

This effort was sponsored by the Space and Missile Systems Organization, Air Force Systems Command under Contract F04701-70-C-0109. The authors express appreciation to the staff of Tunnel F, AEDC, for conducting the test program reported here, and particularly to A. H. Boudreau for supervision and reduction of data.[1]

References

[1] Boudreau, A. H., "Heat Transfer, Pressure, and Force Tests on the SAMSO/GE RVTO-3B Vehicle at Mach 11," Arnold Engineering Development Center, Arnold AFB, Tenn., AEDC-TR-73-85, May 1973.

[2] Bushnell, D. M. and Weinstein, L. M., "Correlation of Peak Heating for Reattachment of Separate Flows," *Journal of Spacecraft and Rockets*, Vol. 5, Sept. 1968, pp. 1111-1112.

[3] Walker, G. K., "Some Comments on Laminar and Turbulent Heat Transfer Equations," GE-MSVD AETM No. 147, Dec. 1959.

[4] Keyes, J. W. and Morris, D. J., "Correlations of Peak Heating in Shock Interference Regions at Hypersonic Speeds," *Journal of Spacecraft and Rockets*, Vol. 9, Aug. 1972, pp. 621-623.

[5] Kaplan, M., "High Speed Boundary Layer Separation in a Compression Corner," General Electric, Philadelphia, Pa., MSVD Thermo. Fundamental Memo TFM-HTT-8151-001, May 1962.

[6] Nestler, D. E., "Correlation of Turbulent Heat Flux to Deceleration Flaps in Supersonic Flow," Paper 68-13, AIAA 6th Aerospace Sciences Meeting, New York, Jan. 1968; also *Journal of Spacecraft and Rockets*, Vol. 5, Aug. 1968, pp. 998-1000.

[7] Holden, M. S., "Shock Wave-Turbulent Boundary Layer Interaction in Hypersonic Flow," AIAA Paper 72-74, Washington, D.C., 1974.

[8] Goldberg, T. J., Ashby, G. C., Jr., and Hondros, J. G., "Centerline Pressure Distributions on Two Dimensional Bodies with Leading Edge Angles Greater Than That for Shock Detachment at Mach Number 6 and Angles of Attack Up to 25°," NASA TN-D-1793, June 1963.

[9] Ashby, G. C., Jr. and Goldberg, T. J., "Application of Generalized Newtonian Theory to Three-Dimensional Sharp-Nose Shock-Detached Bodies at Mach 6 for Angles of Attack Up to 25°," NASA TN-D-2550, Jan. 1965.

[10] Ames Research Staff, "Equations, Tables, and Charts for Compressible Flow," NACA Report 1135, 1953.

[11] Kim, B. S. C. and Parkinson, T. W., "Flap Turbulent Heating Characteristics Obtained from a Hypersonic Shock Tunnel," AIAA Paper 71-598, Washington, D. C., 1971; also *Journal of Spacecraft and Rockets*, Vol. 9, April 1972, pp. 227-229.